Mode-resolved detection of magnetization dynamics using x-ray diffractive ferromagnetic resonance

David M. Burn,[*,†] Shilei Zhang,[*,‡] Kun Zhai,[¶] Yisheng Chai,[§] Young Sun,[¶] Gerrit van der Laan,[*,†] and Thorsten Hesjedal[*,‖]

†*Magnetic Spectroscopy Group, Diamond Light Source, Didcot OX11 0DE, United Kingdom*

‡*School of Physical Science and Technology, ShanghaiTech University, Shanghai, 201210, China; ShanghaiTech Laboratory for Topological Physics, ShanghaiTech University, Shanghai 200031, China*

¶*Beijing National Laboratory for Condensed Matter Physics, Institute of Physics, Chinese Academy of Sciences, Beijing 100190, China; School of Physical Science, University of Chinese Academy of Sciences, Beijing 100190, China*

§*Low Temperature Physics Laboratory, College of Physics, and Center of Quantum Materials and Devices, Chongqing University, Chongqing, 401331, China*

‖*Clarendon Laboratory, Department of Physics, University of Oxford, Parks Road, Oxford, OX1 3PU, United Kingdom*

E-mail: david.burn@diamond.ac.uk; zhangshl1@shanghaitech.edu.cn; Gerrit.vanderLaan@diamond.ac.uk; Thorsten.Hesjedal@physics.ox.ac.uk

Abstract

Collective spin excitations of ordered magnetic structures offer great potential for the development of novel spintronic devices. The present approach is to rely on micromagnetic models to explain the origins of dynamic modes observed by ferromagnetic resonance (FMR) studies, since experimental tools to directly reveal the origins of the complex dynamic behavior are lacking. Here we demonstrate a new approach which combines resonant magnetic x-ray diffraction with FMR, thereby allowing for a reconstruction of the real-space spin dynamics of the system. This new diffractive FMR (DFMR) technique builds on x-ray detected FMR (XFMR) that allows for element-selective dynamic studies, giving unique access to specific wave components of static and dynamic coupling in magnetic heterostructures. In combination with diffraction, FMR is elevated to the level of a modal spectroscopy technique, potentially opening new pathways for the development of spintronic devices.

Keywords: Ferromagnetic resonance, multiferroics, topological spin texture, magnetic phase diagram, resonant elastic x-ray scattering

Innovative magnetic materials have played a pivotal role for the increase in data storage capacity over the past decades, and have lead to the advent of spintronic devices. Especially multilayers in, e.g., giant magnetoresistance or tunneling magnetoresistance structures, contributed significantly as they allow for a precise design of their magnetic properties.[1–3] Recently, topologically ordered magnetic systems, such as skyrmions, and multiferroic materials in which ordered magnetic moments can be manipulated via the application of an electric field, have been the focus of attention as they promise high-density and low-energy-consumption data processing solutions.

Among the various techniques to study the magnetization dynamics of these magnetic systems, such as time-resolved magneto-optical Kerr effect measurements and Brillouin-light scattering,[4] ferromagnetic resonance (FMR) is widely used.[5–8] The most common approaches in FMR use either a broadband coplanar waveguide (CPW) or a resonant cavity design, restricted to the study of the total magnetization only. Magnetic devices, however, consist of several different layers whose properties can only be inferred indirectly by comparing experimental FMR spectra with micromagnetic models.[8] Synchrotron radiation-based x-ray detected FMR (XFMR) was developed to study element-specific magnetization dynamics, thus giving layer-selective resolution of the magneto-dynamics in multilayer samples.[9–19] Magnetic and chemical contrast is provided by the x-ray magnetic circular dichroism (XMCD) effect,[20,21] while the phase difference between the spin precessions can be determined using stroboscopic sampling. However, for complex spin structures such as helical or skyrmion systems, the net magnetization probed by the x-ray beam can vanish, rendering normal XFMR unsuitable. Time-resolved scanning transmission x-ray microscope (STXM),[22] on the other hand, allows for the detection of FMR modes with a spatial resolution down to a scale of $\sim$25 nm.[23] This XMCD-based technique has been successfully used to investigate magnetic nanoscale system such as spin waves generated by a spin torque oscillator,[22] single and coupled nanomagnets,[24] and spin wave excitation and propagation in 1D and 2D.[23]

Resonant elastic x-ray scattering (REXS) in the soft x-ray regime is an ideal tool to

study periodically ordered spin systems. Since the incident x-rays can be chosen as linear or circular polarized all three components of the magnetization vectors can be accessed.[25] In REXS, periodic magnetic (super)structures lead to satellites which appear around the structural peaks in reciprocal space.

Here, we introduce x-ray detected diffractive ferromagnetic resonance (DFMR) as a novel synchrotron radiation-based technique, combining both REXS and FMR, to selectively probe dynamic spin modes from specific periodic features. Magnetic contrast originating from x-ray magnetic circular (or linear) dichroism is probed stroboscopically revealing the time dependence of the magnetization precession. With periodic magnetic structural features providing diffraction peaks in a scattering geometry, the dynamics purely associated with these periodic structures can be uniquely identified. Using the rich magnetic structure of a Y-type hexaferrite as an example, we demonstrate the capabilities of DFMR. With significant interest in chiral and rich topological spin structures for potential technological devices, techniques to probe the dynamics of these systems are of significant importance.

DFMR essentially combines two established techniques in order to study the mode-resolved magnetization dynamics. First, REXS in the soft x-ray regime reveals the *static* magnetic structure in reciprocal space. REXS can be carried out at a synchrotron facility using a diffractometer which provides a variable sample temperature and magnetic field environment in ultrahigh vacuum. Under the diffraction condition the spatial resolution d is determined by the Bragg condition $d = \lambda/(2\sin\theta)$, where θ is the Bragg angle and λ the wavelength which is, e.g., 17.5 Å at the Fe L_3 absorption edge. Second, x-ray detected FMR, which is based on the XMCD effect, gives conventional FMR the ability to probe the element-specific spin *dynamics*. The incident x-rays are tuned to the corresponding $L_{2,3}$ absorption edge of the $3d$ transition metal element of interest. For XFMR, the sample is attached to a coplanar waveguide, placed inside of a variable magnetic field, and excited with microwave radiation. The magnetization dynamics is sampled stroboscopically, i.e., the microwave frequency has to be an integer multiple of the x-ray pulse frequency of the

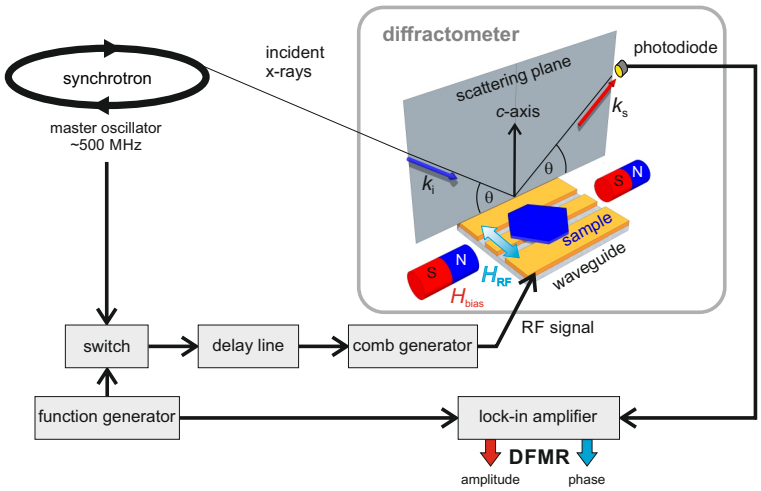

Figure 1: **Diffractive ferromagnetic resonance (DFMR) setup.** The schematic shows the sample placed onto a CPW on the cryostat inside a soft x-ray diffractometer. A magnetic field can be applied in the scattering plane along the CPW. The energy of the incident x-rays is tuned to the Fe L_3 absorption edge of the hexaferrite sample. Static structural and magnetic diffraction peaks are detected with a photodiode. For dynamic measurements, a specific diffraction peak is selected and an amplitude-modulated RF signal (pump) is applied to the sample. The probing x-rays are pulsed at ∼500 MHz, and a comb generator provides higher harmonics of the pulse frequency to the sample. A delay line enables phase shifting of the microwave oscillation with respect to the x-ray pulses. Additionally, VNA-FMR can be measured in the diffractometer (not shown here).

synchrotron of 499.68 MHz (the master oscillator clock of the Diamond storage ring). A delay line allows for a phase shifting of the microwave oscillation with respect to the x-ray pulse. This way, the XMCD can be monitored as a function of the delay between RF excitation (pump) and x-ray bunch arrival (probe), whereby x-ray absorption is often detected in transmission using the optical luminescence of the substrate.[18]

DFMR combines REXS and XFMR by measuring the change in intensity of the scattered peaks resulting from the stroboscopic probing of the magnetic structure. As for XFMR, a microwave signal passing through a coplanar waveguide is used to excite the sample. However, in contrast to XFMR, which uses a transmission geometry, the sample surface has now to face up to allow for the x-rays to scatter. Consequently, the sample has to be suitably thin such that the magnitude of the RF field is sufficiently strong to drive the magnetization dynamics at the sample surface. As for XFMR, the driving RF is phase-locked to an integer multiple of the synchrotron master oscillator clock. This synchronization means that photons probe the sample at specific points in time within the RF excitation waveform, thus providing a stroboscopic measurement of the magnetic state. Using a variable length delay line allows for the measurement of the time evolution of the diffracted intensity. To enhance the signal, the RF signal was amplitude-modulated at 1.9 kHz and the dynamic contributions were detected using a lock-in amplifier. A schematic of the experimental setup is shown in Figure 1.

Hexaferrites are particularly interesting materials for information storage applications since they are magnetic and in some cases multiferroic at room temperature.[26–28] There are three main types of hexaferrites relevant to magnetoelectric phenomena and applications. These are known as M-type, Y-type, and Z-type, having the chemical composition $AFe_{12}O_{19}$, $A_2M_2Fe_{12}O_{22}$, and $A_3M_2Fe_{24}O_{41}$, respectively, where A = Pb, Ca, Sr, Ba and M = transition metal. Here, we demonstrate the abilities of the DFMR technique on the Y-type hexaferrite $Ba_2Mg_2Fe_{12}O_{22}$ (space group $R\bar{3}m$),[29] which has a rich magnetic behavior.[28]

Vector network analyzer (VNA) FMR measurements form an important part of the

precharacterization of systems for DFMR. Broadband VNA-FMR is used for studying the magnetic resonance modes of a sample and to determine the field needed to drive magnetic resonance at the specific frequencies, as required for DFMR. VNA-FMR measurements can also be performed in-situ in the diffractometer. Figure 2a shows the RF absorption of the hexaferrite sample as a function of frequency and applied in-plane bias field (perpendicular to the RF field). The hysteresis loop measured in resonant x-ray diffraction is shown in Figure 2b. Figure 2c shows the two RF resonance modes for a fixed frequency of 6 GHz as a function of magnitude and direction of the applied field. The two modes, labeled A and B, are clearly visible. Mode A is isotropic, i.e., the resonance frequency is independent of the field direction. However, the absorption strength decreases when the bias field is applied parallel to the RF field. Mode B shows much stronger resonant absorption, as well as a pronounced dependence on the applied field direction, especially for out-of-plane directions. Both modes show a non-trivial step behavior as a function of field, indicative of partial switching of the sub-units and transitions between the different magnetic states.[30]

Next, we use resonant soft x-ray diffraction to characterize the static magnetic structure of the hexaferrite and determine its field dependence. Static REXS measurements along (0,0,l) in zero field (Figure 3) show the (0,0,3) structural peak decorated with two incommensurate magnetic satellites, q_1 and q_2, similar to the helical magnetic structure in $Ba_xSr_{1-x}Zn_2Fe_{12}O_{22}$.[31,32] The photon energy scans across the three peaks show that the scattering intensity is largest at the Fe L_3 edge (707.7 eV). The insets to the right of the magnetic q_1 peak and the structural (0,0,3) peak show the field dependence of their scattered intensities from 0 to 167 mT. Whereas the q_1 peak clearly reveals its magnetic origin, with the intensity suppressed at 167 mT, the structural peak is only field dependent up to $\sim$66 mT. The slight reduction at lower fields characterizes the interference of charge and magnetic contributions to the diffraction.

Next, we use DFMR to probe the dynamics of the individual magnetic modes. For this purpose, the intensity of the selected diffraction peak is measured with a photodiode detector.

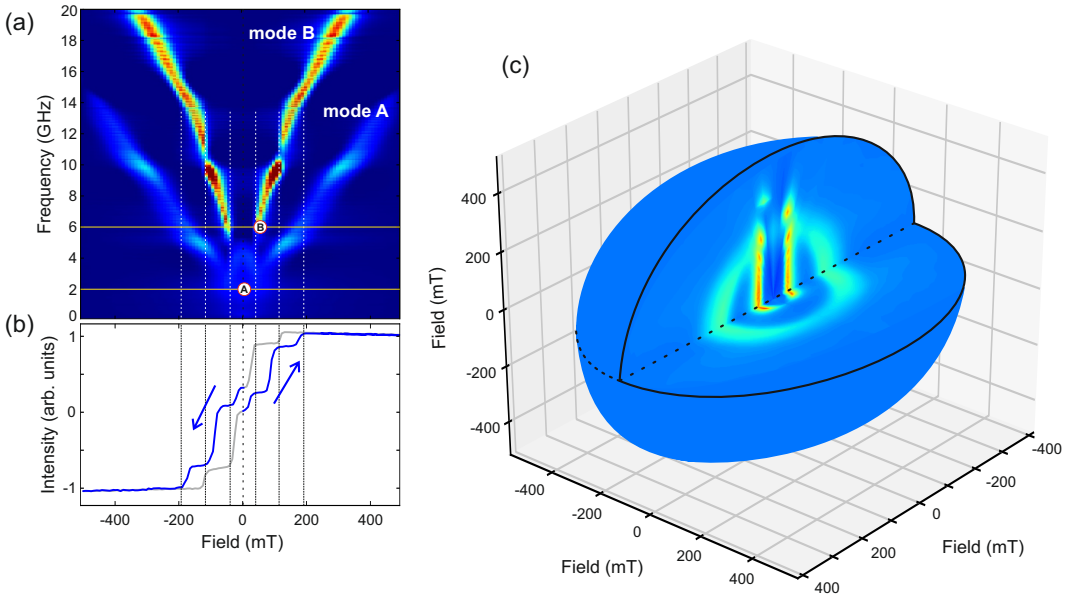

Figure 2: **VNA-FMR measurements.** (a) Frequency-field map of the RF absorption and (b) corresponding hysteresis loop measured by REXS. Two modes A and B are observed, where the red circles indicate the place where DFMR delay scans (Figures 4 and 5) were taken. Step-like transitions in the hysteresis loop are marked by vertical lines, which correspond to features in the frequency-field map. The blue arrows give the direction of the magnetic field sweep. (c) Plot of the absorption as a function of applied field direction and magnitude (at a frequency of 6 GHz) showing the two ferromagnetic resonance modes A and B. Mode A is isotropic, i.e., the field values are independent of the angle of the applied field. The anisotropic mode B shows greater absorption at increasingly higher fields as the field direction rotates out-of-plane.

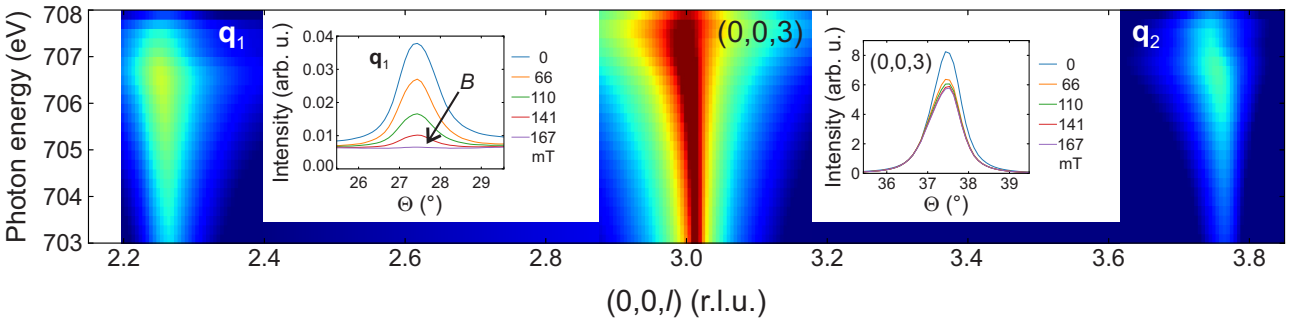

Figure 3: **Resonant elastic x-ray scattering (REXS) in static mode.** REXS intensity as a function of photon energy along the $(0,0,l)$ direction. The structural (0,0,3) peak is decorated by incommensurate, field-dependent magnetic satellites at q_1 and q_2. The scattered intensity is strongest at the Fe L_3 edge at 707.7 eV. As shown in the insets, the magnetic peaks are field dependent (left inset shows the q_1 peak), whereas the structural peak (right inset) is almost field independent above a certain threshold value (∼66 mT).

Figure 4a shows delay scans, i.e., the scattered dynamic signal as a function of time delay between pump and probe. Accumulating delay scans as a function of applied field probes the resonance, which occurs at 55 mT for mode B at 6 GHz (consistent with VNA-FMR results shown in Figure 2). Figures 4a and 4c show the extracted amplitude and phase of the DFMR signal, respectively, obtained by sinusoidal fits to the data. The Lorentzian lineshape in the amplitude is accompanied by a near 180° shift in phase. For the time-resolved REXS measurement, the photodiode was positioned at the diffraction condition for the q_2 magnetic satellite using a linear polarization angle of 55° for the incident x-rays. The DFMR signal shows essentially the change in (stroboscopically) measured REXS intensity at the modulation frequency of the applied RF field. The DFMR signal follows a sinusoidal behavior as a function of the time delay between the x-ray pulse arrival time (probe) and the RF (pump). The period of this oscillation is 166 ps, corresponding to the 6 GHz RF field applied to the sample.

A deeper understanding of the magnetization dynamics of the resonance modes can be achieved by carrying out DFMR on different scattered peaks and also by varying the polarization of the probing x-ray beam.[33] Figure 5 shows the delay scans from the magnetic q_1, the structural (0,0,3), and the magnetic q_2 peaks as a function of the linear polarization angle η, with respect to vertically polarized x-rays ($\eta = 0°$). The DFMR delay scans show a sinusoidal dependence on the delay for all three peaks in Figures 5a and 5b. For all peaks, the intensity as a function of η is sinusoidally modulated, with a period of 180° due to the rotation properties of the linear polarization about the beam direction.

The period of the DFMR delay scans of mode B in Figure 5a is 166 ps (corresponding to an RF frequency of 6 GHz). For the two magnetic satellites q_1 and q_2, the amplitude changes as a function of polarization angle. For vertically and horizontally ($\eta = 90°$) polarized light, a negligible dynamic signal is detected. On the other hand, for $\eta = 45°$ and 135°, there is a strong signal with inverted polarity since the intensity is sinusoidally modulated with η. The dynamics of the magnetic satellites remain at a constant phase and there are negligible

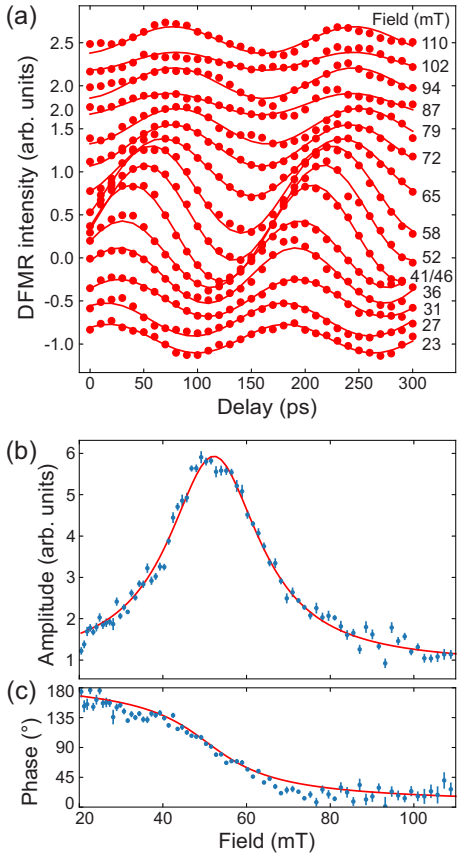

Figure 4: **Field-dependent DFMR.** (a) Delay scans measured on the q_2 peak at 6 GHz as a function of applied field. The incident x-rays were linearly polarized ($\eta = 55°$). The solid lines represent sinusoidal fits to the measured data. The signal amplitude is largest at the resonant field of 55 mT. Extracted field dependence of (b) amplitude and (c) phase of the dynamic signal whilst crossing the resonance. The solid lines are a Lorentzian fit to the amplitude data and a representative arctan function to highlight the phase change.

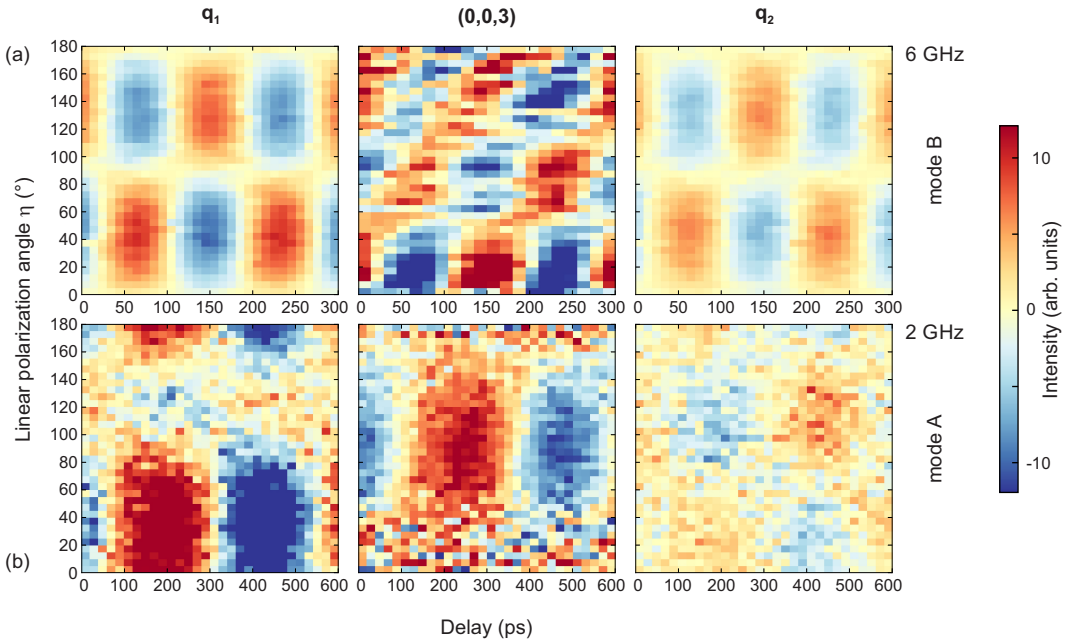

Figure 5: **DFMR delay scans of the structural and magnetic peaks as a function of polarization angle.** Measurements of (a) the anisotropic mode B at 6 GHz and (b) the isotropic mode A at 2 GHz (marked in Figure 2a by the red circles). From left to right the results for the magnetic q_1, the structural (0,0,3), and the q_2 peak are shown. The magnetic resonance modes are probed with linearly polarized light for a range of incident polarization angles η.

differences between the measurements on both satellites.

In contrast, the structural (0,0,3) peak shows a considerably different behavior compared to the magnetic peaks. Overall, there is only a weak variation of the amplitude with linear polarization angle. Nevertheless, approximately three phase regions can be identified, between which a phase jump occurs as a function of linear polarization angle. Note that the complex DFMR signal of the structural (0,0,3) peak contains information about every dynamic behavior that repeats with the periodicity of the unit cell, i.e., magnetic and charge interference related,[25] whereas the magnetic satellites only reflect the dynamics of the magnetization that exists at the conical modulation period within this structure. This way, DFMR provides a means to separate the coexisting contributions to the magnetization dynamics of a complex spin system.

The other ferromagnetic resonance mode (mode A) shows a very different dynamic behavior compared to mode B. Figure 5b shows the equivalent DFMR delay scans on the three diffractive peaks whilst the system was driven in the ferromagnetic resonance mode at 2 GHz in a field of 5 mT. At this RF frequency, the periodicity of the sinusoidal delay scans is 500 ps (as seen for all three diffraction peaks). For both magnetic peaks in mode A, the amplitude is again modulated with η, however, in more complex way. For q_1 a large signal is detected from 170° to (180°+) 90°, consistent with a sinusoidal dependence on η, however, now offset from zero. For q_2, a somewhat larger signal is confined to 80-140°, now with an opposite offset. In contrast to mode B, the DFMR measured on the structural (0,0,3) peak for mode A in Figure 5b shows no variation in phase with polarization angle.

REXS measured with linear polarization of the incident beam is sensitive to the components of the magnetic moments in and out of the scattering plane. The magnetic Bragg peaks originate from pure magnetic scattering with intensity given by Eq. (17) of Ref.[25] The structural Bragg peaks arise from charge scattering as well as charge-magnetic interference scattering with intensities given by Eqs. (16) and (18), respectively, in Ref.,[25] and hence show a rather different behavior. For a fixed scattering geometry of a magnetic peak,

varying the incident polarization angle corresponds to probing different components of the three-dimensional magnetization vector. By varying η from 0-180°, DFMR provides insight into the time-dependence of the precession of the magnetization vector, superimposed onto the static conical magnetic structure. For mode B, the η-dependent sinusoidal variation of the DFMR signal suggests a directional dependence of the time-dependent precessional dynamics which does not average out to zero over the spins that make up the repetition in the conical structure. For mode A, an additional offset in the DFMR signal suggests a direction-independent contribution to the precession, which exists in combination with a sinusoidal dependence similar to that seen in mode B. These features are consistent with the VNA-FMR data.

Y-type hexaferrite $BaSrMg_2Fe_{12}O_{22}$ exhibits a complex magnetic structure. In terms of its magnetic properties, the unit cell can be seen as a sequence of large (L) and small spin moment (S) blocks (L and S moments shown in blue and red, respectively, in Figure 6a). Within these blocks, the magnetic moments are lying in the *ab*-plane. Across the boundary between L and S blocks, the Fe atoms couple by superexchange interaction via an oxygen atom. Neighboring (large) Ba and (small) Sr atoms affect this superexchange trio by altering the bond angle. The combination of these coupling effects results in a variety of magnetic structures such as collinear ferrimagnetic (Figure 6b), proper screw (Figure 6c), and transverse conical state (Figure 6d,e).[26,34]

Figures 6b-e show the simulation results for linear polarization-dependent DFMR delay scans for these magnetic structures in Y-type $BaSrMg_2Fe_{12}O_{22}$.[26] The DFMR simulations of their normal modes were carried out using our method outlined in Ref.,[33] effectively taking into account the phase differences between the moments. For the transverse conical state, two modes can be excited, i.e., a lower energy in-phase mode A and a higher energy out-of-phase mode B (with the phase varying by 2π over a full period of the magnetic structure). As can be seen, none of the simulated DFMR contrasts is able to fully describe the experimental data shown in Figure 5. This finding highlights the complexity of the dynamic properties of

well-known static structures, suggesting that the simple resonant mode model is incomplete. It is, however, clear that DFMR is very sensitive to the dynamic properties, as evidenced by the distinctly different DFMR delay scan contrasts for the A and B modes shown in Figures 6d and 6e, which are obtained for identical static magnetic structures (transverse conical).

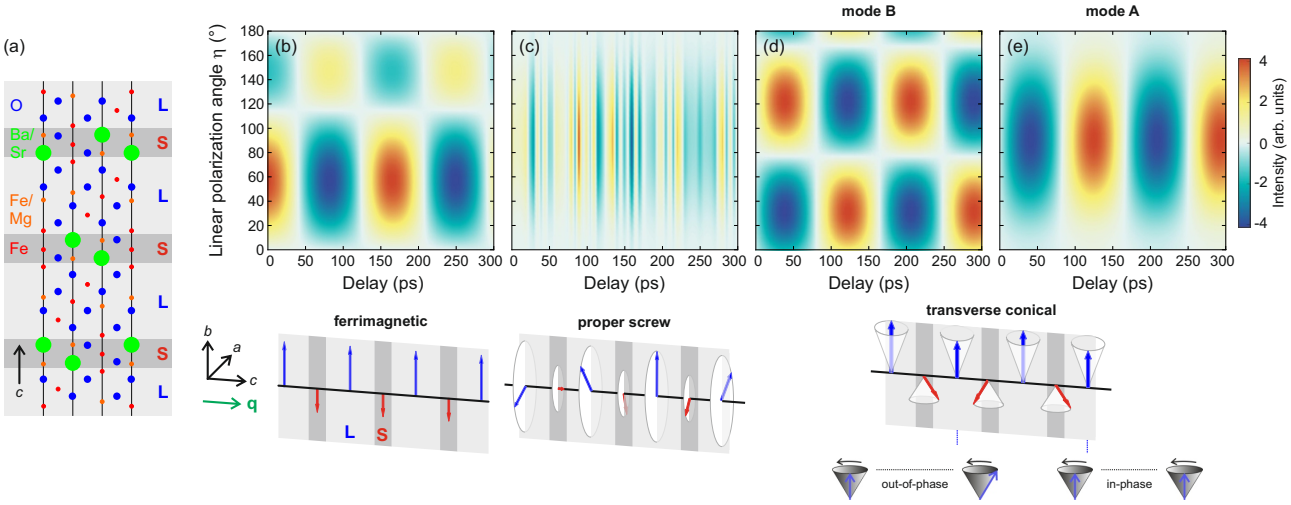

Figure 6: **Simulation of linear polarization-dependent DFMR delay scans for common magnetic structures in Y-type $BaSrMg_2Fe_{12}O_{22}$.** (a) Illustration of the crystal structure and the alternating L and S blocks (light and dark gray). Blue arrows represent the magnetic moment of the L blocks and red arrows the S blocks. Simulated DFMR delay scans for (b) the ferrimagnetic, (c) the proper screw, and (d,e) the transverse conical state for (d) mode B and (e) mode A. Below, the respective static magnetization structures are shown.

In conclusion we demonstrate a novel experimental technique for probing magnetization dynamics arising from different spatial frequencies within magnetic material systems. The power of x-ray detected ferromagnetic resonance is combined with that of resonant elastic x-ray scattering, giving dynamic information of specific magnetically ordered periodic phases. The data collected as a function of linear polarization of the x-rays enables us to extract the microscopic information of the magnetization dynamics. We demonstrate the ability of DFMR to study distinct magnetic phases through measurements on Y-type hexaferrite which contains a rich level of complexity. The use of this technique applied to further magnetic systems will allow complex magnetic dynamic processes to be interrogated in the future.

Sample Preparation. Single crystals of $Ba_2Mg_2Fe_{12}O_{22}$ were prepared by crystallization from high-temperature Na_2O-Fe_2O_3 flux melted at 1420°C in a Pt crucible and slowly cooled to 1100°C after a thermal recycle. The as-grown crystals were characterized by both x-ray diffraction and SQUID magnetometry.

Ferromagnetic resonance (FMR). Prior to the synchrotron experiments, the samples were characterized using coplanar waveguide VNA-FMR, both in the diffraction chamber and in a dedicated octupole magnet system. The vector network analyzer was used to measure the scattering parameters S representing the absorption of an RF excitation by the magnetic system. In particular, two-dimensional f-B maps of S_{21} were obtained as a function of RF frequency, f, and applied field, $\mathbf{B}$.[35] (see Figure 2) These results were used to select the appropriate parameters for the DFMR experiment and to demonstrate consistency with off-line VNA-FMR studies on similar systems.

Diffractive ferromagnetic resonance (DFMR). A high quality $Ba_2Mg_2Fe_{12}O_{22}$ sample measuring $2 \times 2 \times 0.1$ mm^3 was mounted with the sample normal $\parallel$ c-axis onto the cryostat finger of the ultra-high vacuum RASOR diffractometer on beamline I10 at the Diamond Light Source, UK.[36] The beam spot size at the sample position is typically 100×100 μm^2, thereby avoiding the effects of non-uniform microwave excitation.[8] The sample can be cooled to 12 K while a variable magnetic bias field can be applied in the scattering plane. Here, this bias field was applied in the plane of the sample, which was kept at room temperature. A small microwave field perpendicular to the bias field is applied to drive the magnetization in precession at its resonance frequency. The DFMR experiments were performed using linearly polarized soft x-rays with variable polarization angle, and with the energy tuned to the Fe L_3 absorption edge at 707.7 eV. The detector slits provide an angular resolution of 3 mrad. DFMR measures the variation in intensity of the scattered peaks resulting from the stroboscopic probing of the magnetic structure with a pulsed x-ray source synchronized

with magnetic dynamic processes. For this purpose, we used the 900-bunch operation mode at the Diamond Light Source, providing pulsed photon bunches (41.5 ± 0.2) ps FWHM at a repetition frequency of the synchrotron master clock (499.68 MHz).[37] For the stroboscopic measurements, the microwave frequency has to be a harmonic of the x-ray pulse frequency, hence the resonance is driven at multiples of the clock frequency, corresponding to a $\sim$2 ns interval between consecutive x-ray pulses. Using filters and subsequent amplifiers, the CPW is excited by a narrow band, high power microwave field of 25-30 dBm. The phase shifting of the microwave oscillation with respect to the x-ray pulses is accomplished with a programmable delay line (time step resolution 0.5 ps). The pulse width of the x-rays ($\sim$41 ps) is limiting the maximum DFMR frequency to $\sim$15 GHz,[38] and it is further reduced by microwave losses to $\sim$11 GHz. The timing jitter of the master oscillator signal at the Diamond synchrotron measured using a spectrum analyzer at the beamline was found to be negligible. Note, however, that in the stroboscopic measurement the jitter ultimately determines the time resolution, not the x-ray pulse width. Finally, the real and imaginary parts of the DFMR signal (or the amplitude and phase) were extracted using audio frequency modulation (1.9 kHz) and lock-in detection.

Acknowledgment

The DFMR experiments were carried out in RASOR on beamline I10 at the Diamond Light Source (Oxfordshire, UK) under proposal SI18898. S. L. Z. acknowledges a starting grant from ShanghaiTech University. Financial support through the Engineering and Physical Sciences Research Council (EPSRC) under grant EP/N032128/1 is gratefully acknowledged.

Author Contributions

The method was conceived and the experiments were designed and carried out by D. M. B., S. L. Z., G. v. d. L., and T. H. The samples were prepared by K. Z., Y. C., and Y. S, while D. M. B., S. L. Z., G. v. d. L., and T. H. contributed to the data analysis, discussions, and writing of the manuscript.

Notes

The authors declare no competing financial interest.

References

(1) Suess, D.; Schrefl, T.; Fahler, S.; Kirschner, M.; Hrkac, G.; Dorfbauer, F.; Fidler, J. Exchange spring media for perpendicular recording. *Appl. Phys. Lett.* **2005**, *87*, 012504.

(2) Suess, D.; Schrefl, T.; Dittrich, R.; Kirschner, M.; Dorfbauer, F.; Hrkac, G.; Fidler, J. Exchange spring recording media for areal densities up to 10 Tbit/in^2. *J. Magn. Magn. Mater.* **2005**, *290*, 551–554.

(3) Victora, R.; Shen, X. Composite media for perpendicular magnetic recording. *IEEE Trans. Magn.* **2005**, *41*, 537–542.

(4) Bland, J. A. C.; Heinrich, B. *Ultrathin Magnetic Structures I. An Introduction to the Electronic, Magnetic and Structural Properties*; Springer-Verlag Berlin Heidelberg, 1994.

(5) Cochran, J.; Heinrich, B.; Arrott, A. Ferromagnetic-resonance in a system composed of a ferromagnetic substrate and an exchange-coupled thin ferromagnetic overlayer. *Phys. Rev. B* **1986**, *34*, 7788–7801.

(6) Metaxas, P. J.; Stamps, R. L.; Jamet, J.-P.; Ferre, J.; Baltz, V.; Rodmacq, B.; Politi, P. Dynamic binding of driven interfaces in coupled ultrathin ferromagnetic layers. *Phys. Rev. Lett.* **2010**, *104*, 237206.

(7) Magaraggia, R.; Kennewell, K.; Kostylev, M.; Stamps, R. L.; Ali, M.; Greig, D.; Hickey, B. J.; Marrows, C. H. Exchange anisotropy pinning of a standing spin-wave mode. *Phys. Rev. B* **2011**, *83*, 054405.

(8) Kaiser, A. M.; Schoeppner, C.; Roemer, F. M.; Hassel, C.; Wiemann, C.; Cramm, S.; Nickel, F.; Grychtol, P.; Tieg, C.; Lindner, J.; Schneider, C. M. Nano and picosecond magnetization dynamics of weakly coupled CoFe/Cr/NiFe trilayers studied by a multitechnique approach. *Phys. Rev. B* **2011**, *84*, 134406.

(9) Goulon, J.; Rogalev, A.; Wilhelm, F.; Jaouen, N.; Goulon-Ginet, C.; Goujon, G.; Youssef, J. B.; Indendom, M. V. X-ray detected magnetic resonance at the Fe K-edge in YIG: forced precession of magnetically polarized orbital components. *JETP Lett.* **2005**, *82*, 696–701.

(10) Guan, Y.; Bailey, W.; Kao, C.; Vescovo, E.; Arena, D. Comparison of time-resolved x-ray magnetic circular dichroism measurements in reflection and transmission for layer-specific precessional dynamics measurements. *J. Appl. Phys.* **2006**, *99*, 08J305.

(11) Martin, T.; Woltersdorf, G.; Stamm, C.; Duerr, H. A.; Mattheis, R.; Back, C. H.; Bayreuther, G. Layer resolved magnetization dynamics in interlayer exchange coupled

$Ni_{81}Fe_{19}$/Ru/$Co_{90}Fe_{10}$ by time resolved x-ray magnetic circular dichroism. *J. Appl. Phys.* **2008**, *103*, 07B112.

(12) Boero, G.; Mouaziz, S.; Rusponi, S.; Bencok, P.; Nolting, F.; Stepanow, S.; Gambardella, P. Element-resolved x-ray ferrimagnetic and ferromagnetic resonance spectroscopy. *New J. Phys.* **2008**, *10*, 013011.

(13) Goulon, J.; Rogalev, A.; Wilhelm, F.; Goujon, G.; Brouder, C.; Yaresko, A.; Ben Youssef, J.; Indenbom, M. V. X-ray detected magnetic resonance of YIG thin films in the nonlinear regime of spin waves. *J. Magn. Magn. Mater.* **2010**, *322*, 2308–2329.

(14) Arena, D. A.; Ding, Y.; Vescovo, E.; Zohar, S.; Guan, Y.; Bailey, W. E. A compact apparatus for studies of element and phase-resolved ferromagnetic resonance. *Rev. Sci. Instrum.* **2009**, *80*, 083903.

(15) Marcham, M. K.; Keatley, P. S.; Neudert, A.; Hicken, R. J.; Cavill, S. A.; Shelford, L. R.; van der Laan, G.; Telling, N. D.; Childress, J. R.; Katine, J. A.; Shafer, P.; Arenholz, E. Phase-resolved x-ray ferromagnetic resonance measurements in fluorescence yield. *J. Appl. Phys.* **2011**, *109*, 07D353.

(16) Marcham, M. K.; Shelford, L. R.; Cavill, S. A.; Keatley, P. S.; Yu, W.; Shafer, P.; Neudert, A.; Childress, J. R.; Katine, J. A.; Arenholz, E.; Telling, N. D.; van der Laan, G.; Hicken, R. J. Phase-resolved x-ray ferromagnetic resonance measurements of spin pumping in spin valve structures. *Phys. Rev. B* **2013**, *87*, 180403.

(17) Bailey, W. E.; Cheng, C.; Knut, R.; Karis, O.; Auffret, S.; Zohar, S.; Keavney, D.; Warnicke, P.; Lee, J.-S.; Arena, D. A. Detection of microwave phase variation in nanometre-scale magnetic heterostructures. *Nat. Commun.* **2013**, *4*, 2025.

(18) Baker, A. A.; Figueroa, A. I.; Collins-McIntyre, L. J.; van der Laan, G.; Hesjedal, T. Spin pumping in Ferromagnet-Topological Insulator-Ferromagnet Heterostructures. *Sci. Rep.* **2015**, *5*, 7907.

(19) van der Laan, G. Time-resolved X-ray detected ferromagnetic resonance of spin currents. *J. Electron Spectrosc. Relat. Phenom.* **2017**, *220*, 137.

(20) van der Laan, G.; Thole, B. Strong magnetic-x-ray dichroism in 2p absorption-spectra of 3d transition-metal ions. *Phys. Rev. B* **1991**, *43*, 13401–13411.

(21) van der Laan, G.; Figueroa, A. I. X-ray magnetic circular dichroism - A versatile tool to study magnetism. *Coord. Chem. Rev.* **2014**, *277-278*, 95–129.

(22) Bonetti, S.; Kukreja, R.; Chen, Z.; Spoddig, D.; Ollefs, K.; Schöppner, C.; Meckenstock, R.; Ney, A.; Pinto, J.; Houanche, R.; Frisch, J.; Stöhr, J.; Dürr, H. A.; Ohldag, H. Microwave soft x-ray microscopy for nanoscale magnetization dynamics in the 5-10 GHz frequency range. *Rev. Sci. Instrum.* **2015**, *86*, 093703.

(23) Sluka, V. et al. Emission and propagation of 1D and 2D spin waves with nanoscale wavelengths in anisotropic spin textures. *Nat. Nanotechnol.* **2019**, *14*, 328–333.

(24) Schaffers, T.; Meckenstock, R.; Spoddig, D.; Feggeler, T.; Ollefs, K.; Schöppner, C.; Bonetti, S.; Ohldag, H.; Farle, M.; Ney, A. The combination of micro-resonators with spatially resolved ferromagnetic resonance. *Rev. Sci. Instrum.* **2017**, *88*, 093703.

(25) van der Laan, G. Soft X-ray resonant magnetic scattering of magnetic nanostructures. *C. R. Physique* **2008**, *9*, 570–584.

(26) Kimura, T. Magnetoelectric Hexaferrites. *Ann. Rev. Cond. Matter* **2012**, *3*, 93–110.

(27) Zhai, K.; Wu, Y.; Shen, S.; Tian, W.; Cao, H.; Chai, Y.; Chakoumakos, B. C.; Shang, D.; Yan, L.; Wang, F.; Sun, Y. Giant magnetoelectric effects achieved by tuning spin cone symmetry in Y-type hexaferrites. *Nature Commun.* **2017**, *8*, 519.

(28) Chmiel, F. P.; Prabhakaran, D.; Steadman, P.; Chen, J.; Fan, R.; Johnson, R. D.; Radaelli, P. G. Magnetoelectric domains and their switching mechanism in a Y-type hexaferrite. *Phys. Rev. B* **2019**, *100*, 104411.

(29) Ishiwata, S.; Taguchi, Y.; Murakawa, H. Low Magnetic-Field Control of Electric Polarization Vector in a Helimagnet. *Science* **2008**, *319*, 1643.

(30) Nakajima, T.; Tokunaga, Y.; Matsuda, M.; Dissanayake, S.; Fernandez-Baca, J.; Kakurai, K.; Taguchi, Y.; Tokura, Y.; Arima, T.-h. Magnetic structures and excitations in a multiferroic Y-type hexaferrite $BaSrCo_2Fe_{11}AlO_{22}$. *Phys. Rev. B* **2016**, *94*, 195154.

(31) Mulders, A. M.; Lawrence, S. M.; Princep, A. J.; Staub, U.; Bodenthin, Y.; García-Fernández, M.; Garganourakis, M.; Hester, J.; Macquart, R.; Ling, C. D. Circularly polarized soft x-ray diffraction study of helical magnetism in hexaferrite. *Phys. Rev. B* **2010**, *81*, 092405.

(32) Hiraoka, Y.; Tanaka, Y.; Kojima, T.; Takata, Y.; Oura, M.; Senba, Y.; Ohashi, H.; Wakabayashi, Y.; Shin, S.; Kimura, T. Spin-chiral domains in $Ba_{0.5}Sr_{1.5}Zn_2Fe_{12}O_{22}$ observed by scanning resonant x-ray microdiffraction. *Phys. Rev. B* **2011**, *84*, 064418.

(33) Zhang, S. L.; van der Laan, G.; Hesjedal, T. Direct experimental determination of spiral spin structures via the dichroism extinction effect in resonant elastic soft x-ray scattering. *Phys. Rev. B* **2017**, *96*, 094401.

(34) Tokura, Y.; Kida, N. Dynamical magnetoelectric effects in multiferroic oxides. *Philos. Trans. Royal Soc. A* **2011**, *369*, 3679.

(35) Stenning, G. B. G.; Bowden, G. J.; Maple, L. C.; Gregory, S. A.; Sposito, A.; Eason, R. W.; Zheludev, N. I.; de Groot, P. A. J. Magnetic control of a meta-molecule. *Opt. Express* **2013**, *21*, 1456–1464.

(36) Beale, T. A. W.; Hase, T. P. A.; Iida, T.; Endo, K.; Steadman, P.; Marshall, A. R.; Dhesi, S. S.; van der Laan, G.; Hatton, P. D. RASOR: An advanced instrument for soft x-ray reflectivity and diffraction. *Rev. Sci. Instrum.* **2010**, *81*.

(37) Martin, I. P. S.; Apollonio, M.; Fielder, R. T.; Singh, B. Characterization of the double-double bend achromat lattice modification to the Diamond Light Source storage ring. *Phys. Rev. Accel. Beams* **2018**, *21*, 60701.

(38) Thomas, C. A.; Rehm, G.; Owen, H. L.; Wyles, N. G.; Botchway, S. W.; Schlott, V.; Wahl, M. Bunch purity measurements for diamond. *Nucl. Instrum. Methods Phys. Res. A* **2006**, *566*, 762–6.

For TOC Only

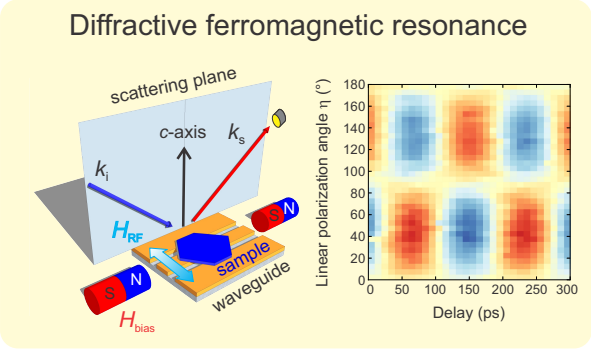

Table of Contents graphic - FOR TOC ONLY